



**HAL**  
open science

# Quantification and mitigation of the effect of resynchronization errors in ultrasound sensor network for passive imaging in elastic plates

Omar Bouchakour, Emmanuel Moulin, Lynda Chehami, Nikolay Smagin

► **To cite this version:**

Omar Bouchakour, Emmanuel Moulin, Lynda Chehami, Nikolay Smagin. Quantification and mitigation of the effect of resynchronization errors in ultrasound sensor network for passive imaging in elastic plates. *Journal of the Acoustical Society of America*, 2024, 155 (5), pp.3283 - 3290. 10.1121/10.0025986 . hal-04607244

**HAL Id: hal-04607244**

**<https://hal.science/hal-04607244v1>**

Submitted on 10 Jun 2024

**HAL** is a multi-disciplinary open access archive for the deposit and dissemination of scientific research documents, whether they are published or not. The documents may come from teaching and research institutions in France or abroad, or from public or private research centers.


L'archive ouverte pluridisciplinaire **HAL**, est destinée au dépôt et à la diffusion de documents scientifiques de niveau recherche, publiés ou non, émanant des établissements d'enseignement et de recherche français ou étrangers, des laboratoires publics ou privés.



Distributed under a Creative Commons Attribution 4.0 International License

MAY 15 2024

# Quantification and mitigation of the effect of resynchronization errors in ultrasound sensor network for passive imaging in elastic plates

Omar Bouchakour; Emmanuel Moulin; Lynda Chehami; Nikolay Smagin 

 Check for updates

*J. Acoust. Soc. Am.* 155, 3283–3290 (2024)

<https://doi.org/10.1121/10.0025986>




WE BRING THE NOISE,  
YOU BRING THE PRODUCTS

COMMITTED TO A SMARTER,  
MORE CONNECTED FUTURE

 **ETS-LINDGREN**  
An ESCO Technologies Company

## Quantification and mitigation of the effect of resynchronization errors in ultrasound sensor network for passive imaging in elastic plates

Omar Bouchakour, Emmanuel Moulin,<sup>a)</sup> Lynda Chehami, and Nikolay Smagin 

Université Polytechnique Hauts-de-France, Université Polytechnique Hauts-de-France, Centre National de Recherche Scientifique, Université de Lille, Unité Mixte de Recherche 8520, Institut d'Electronique de Microélectronique et de Nanotechnologie, F-59313 Valenciennes, France

### ABSTRACT:

The problem of signal desynchronization in passive imaging based on noise correlation for defect detection in elastic plates is investigated. Although a post-processing resynchronization process relying on the symmetry of noise correlation functions can be applied prior to the imaging algorithm, perfect synchronization might not be achieved experimentally. Effect of such residual synchronization errors on the defect detection performance is quantified as a function of their probability density function. A mathematical regularization process is then proposed to reduce the standard deviation of the resynchronization errors by a factor of  $\sqrt{N-1}/N$  ( $N$  is the number of sensors), which results in a significant improvement in the detection performance. Finally, these theoretical results are validated through a simple flexural-wave propagation simulation. © 2024 Acoustical Society of America.

<https://doi.org/10.1121/10.0025986>

(Received 14 December 2023; revised 9 April 2024; accepted 22 April 2024; published online 15 May 2024)

[Editor: Peter Huthwaite]

Pages: 3283–3290

### I. INTRODUCTION

Structural health monitoring (SHM) is attracting strong interest in the industrial community and the subject of active international research. Pitch-catch<sup>1</sup> is one of the most widely used classical ultrasonic methods for defect detection. This kind of so-called “active” method requires controlled sources and, therefore, complex electronics. This might not be practical in some applications, especially SHM-related ones, using embedded sensor networks. A few years ago, some research work<sup>2,3</sup> has performed on Green’s functions, retrieving from ambient noise cross correlation in complex mediums. In the particular case of reverberating plates, noise cross correlation can be written as<sup>4</sup>

$$C(t) \approx [G(t) - G(-t)] \otimes f(t), \quad (1)$$

where  $G(t)$  is the Green’s function,  $f(t) = C_0(t) \otimes K(t)$ ,  $C_0$  is the noise auto-correlation, and  $K(t)$  is a function depending on the plate characteristics.<sup>4</sup>

This made it possible to take advantage of the cross correlation of ambient noise for passive imaging to locate defects in reverberating plates for SHM applications.<sup>5,6</sup> However, this technique requires that signals recorded by the different sensors must be synchronized with each other. This involves an electronic complexity, which might become a real challenge for embedded applications based on wireless sensors network imaging.<sup>7,8</sup>

Coming back to the literature, a set of synchronization methods for sensor networks have been developed and

tested. Arceo-Miquel *et al.*<sup>9</sup> proposed a synchronization approach using an external clock via Global Positioning System (GPS). However, this kind of method may not be accurate, especially when the connection to the external clock fails. Moreover, it is not applicable in certain environments such as underwater, indoors, and under foliage.<sup>10</sup> In Ref. 11, Elson *et al.* developed a synchronization protocol called reference-broadcast synchronization (RBS). The basic idea of such a protocol is that nodes in the network periodically send beacon messages to their neighbors using broadcast at the physical layer. Recipients use the message’s arrival time as a reference point to compare their clocks. However, convergence time and complexity are the major issues of the RBS method. Indeed, it requires a lot of synchronization rounds to achieve reasonable convergence. In addition, each node must communicate with all the other nodes of its neighborhood to achieve convergence.<sup>12</sup> In passive imaging based on noise correlation (in particular, seismology<sup>13,14</sup> and underwater acoustics<sup>15–17</sup> domains), the peak correlation technique (PCT) has been used as a promising method for the detection of signals time shifts. Such an approach is based on the symmetry of the cross-correlation functions.<sup>18</sup> In fact, the correlation between the positive and negative time lags of the cross correlation between signals recorded by a pair of sensors gives a peak of resemblance corresponding to the time shift of this cross correlation. This allows sensor resynchronization in post-processing without adding electronic hardware complexity. However, in the presence of an additive noise during the measurement processes, estimating time shifts using such a technique can lead to resynchronization errors and then a subsequent

<sup>a)</sup>Email: emmanuel.moulin@uphf.fr

degradation of the localization image contrast. The main objective of this work is to quantify this degradation as a function of the standard deviation of the resynchronization error. Then, we show that this error can be reduced by means of a pseudo-inversion process.

This paper is outlined as follows. In Sec. II, the degradation of the contrast ratio of the localization image is quantified as a function of the statistical properties of the resynchronization error. In Sec. III, we show how the resynchronization error can be reduced using a Moore-Penrose pseudo-inversion process. In Sec. IV, the theoretical derivations are validated using a numerical simulation and obtained results are discussed.

## II. INFLUENCE OF SYNCHRONIZATION ERRORS ON DEFECT DETECTION

Let us consider a set of  $N$  independent acoustic sensors attached to a plate subject to some ambient noise. The procedure that we use to detect and localize a possible defect is based on cross-correlating noise recorded at each receiver and applying a backpropagation and dispersion-compensation algorithm. Indeed, as detailed in previous work,<sup>4,5</sup> the computed positive time lag of differential noise cross correlation between two states with and without defect allows to isolate the defect signature. A pixel-by-pixel backpropagation process then allows to build a localization image of the defect.

Here, we will consider that each receiver is driven by its own independent internal clock, leading to possible time drifts between recorded signals. In that case, resynchronization of signals is needed before applying the localization algorithm. In this section, we will investigate the effect of possible residual errors in the resynchronization process on the defect detection performance.

We note  $s_i(t)$  as the signal that would be recorded at the  $i$ th receiver,  $R_i$ , in the case where all receivers are synchronized to a common timebase.

By defining  $\Delta_i$  as the possible clock drift affecting receiver  $R_i$ , we can then write the actually measured signals as

$$s_i^{\text{mes}}(t) = s_i(t - \Delta_i), \quad (2)$$

where  $s_i(t)$  is the signal recorded by  $R_i$  if the receivers were synchronized, and the upper index, “mes,” refers to *measured*.

The cross correlation computed between two receivers,  $R_i$  and  $R_j$ , is then

$$C_{ij}^{\text{mes}}(t) = s_i^{\text{mes}}(t) \otimes s_j^{\text{mes}}(-t), \quad (3)$$

where  $\otimes$  denotes convolution.

Equations (2) and (3) yield

$$C_{ij}^{\text{mes}}(t) = C_{ij}(t - \delta_{ij}), \quad (4)$$

where  $C_{ij}(t) = s_i(t) \otimes s_j(-t)$ , and  $\delta_{ij}$  is the time shift between  $R_i$  and  $R_j$ , which is defined as

$$\delta_{ij} = \Delta_i - \Delta_j. \quad (5)$$

These, supposedly unknown, time shifts have to be estimated so that they can be compensated before applying the localization algorithm. This can be performed by using the PCT, consisting of exploiting the time symmetry that should characterize the quality of Green’s functions reconstruction.<sup>13–17</sup> For that, we compute the cross correlation between  $C_{ij}^{\text{mes}}(t)$  and its time-reversed version. The obtained correlation peak, which would theoretically correspond to the zero time lag of the noise correlation  $C_{ij}(t)$ , is actually obtained at the shifted time lag,  $2\delta_{ij}$  [see Fig. 1(a)]. Then, the measured cross correlation can be resynchronized in post-processing by simply compensating the time shift as follows:

$$C_{ij}^{\text{res}}(t) = C_{ij}^{\text{mes}}(t + \delta_{ij}), \quad (6)$$

where the upper index, “res,” refers to *resynchronized*.

From Eq. (4), this yields

$$C_{ij}^{\text{res}}(t) = C_{ij}(t). \quad (7)$$

However, in the presence of an additive noise in the measurement process, some uncertainties can affect the estimation of the cross-correlation time shifts [see Fig. 1(b)]. The corresponding estimated shift, denoted by  $\delta_{eij}$ , can then be written as

$$\delta_{eij} = \delta_{ij} + \mathcal{E}_{ij}, \quad (8)$$

where  $\mathcal{E}_{ij}$  is the estimation error.

Consequently, the resynchronized cross correlation with  $\delta_{eij}$  can be written as

$$C_{ij}^{\text{res}}(t) = C_{ij}^{\text{mes}}(t + \delta_{eij}), \quad (9)$$

which, according to Eqs. (4) and (8), can be expressed as

$$C_{ij}^{\text{res}}(t) = C_{ij}(t + \mathcal{E}_{ij}). \quad (10)$$

Similar to Eq. (1), positive time lag of the differential cross correlation (subtraction with and without defect) used for imaging can be written as

$$\Delta C_{ij}^+(t) = \Delta G_{ij}(t) \otimes f(t), \quad (11)$$

where  $\Delta G_{ij}(t)$  is the part of the Green’s function resulting from the defect.

In the frequency domain, this yields

$$\Delta C_{ij}^+(\omega) = \Delta G_{ij}(\omega) F(\omega) = \Delta G_{ij}(\omega) C_0(\omega) K(\omega), \quad (12)$$

where  $C_0(\omega)$  is the noise power spectral density and  $K(\omega)$  is the Fourier transform of  $K(t)$ , which is defined in Eq. (1).

In the far-field,  $\Delta G_{ij}(\omega)$  can be written as<sup>19</sup>

$$\Delta G_{ij}(\omega) = B(\omega) f(\theta_{ij}, \omega) \chi_{ij} e^{-jk(\omega)d_{ij}}, \quad (13)$$

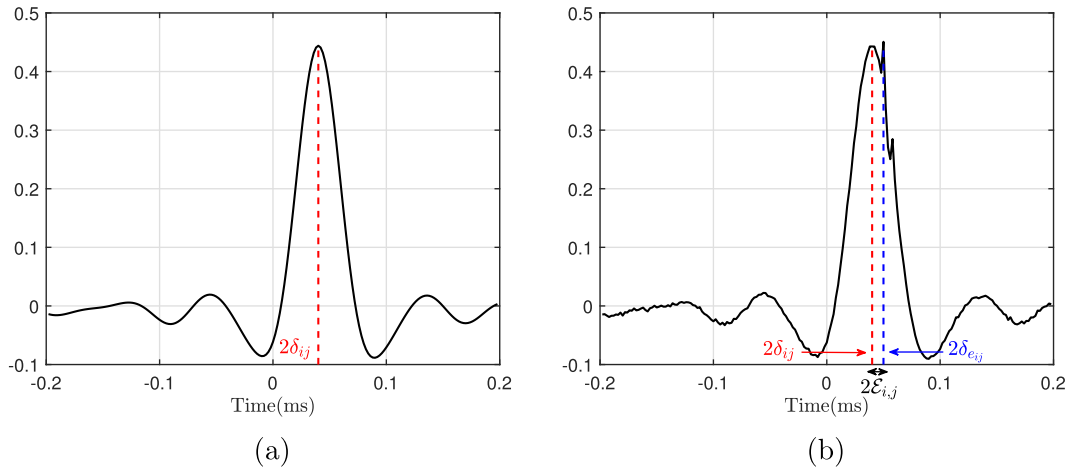


FIG. 1. (Color online) Illustration of an example of the correlation between the positive and negative time lags of  $C_{ij}^{mes}(t)$  windowed around the resemblance peak (a) noise-free case and (b) noisy case.

where  $B(\omega)$  is a frequency-dependent function characterizing the source nature [for example, displacement source if  $B(\omega)$  is constant or load source if  $B(\omega)$  is as given in Ref. 19];  $f(\theta_{ij}, \omega)$  is the scattering amplitude;  $\theta_{ij}$  is the angle of the wave packet scattered by the defect toward  $R_j$  when  $R_i$  is considered as a source;  $\chi_{ij} = 1/\sqrt{d_{id}d_{dj}}$  is a geometric factor, where  $d_{id}$  and  $d_{dj}$  are the distances from  $R_i$  to the defect and the defect to  $R_j$ , respectively;  $d_{ij} = d_{id} + d_{dj}$ ; and  $k(\omega)$  is the wave number that obeys the dispersion relation of the  $A_0$  Lamb mode.

Equations (12) and (13) yield

$$\Delta C_{ij}^+(\omega) = f(\theta_{ij}, \omega) \chi_{ij} e^{-jk(\omega)d_{ij}} U_0(\omega), \quad (14)$$

where  $U_0(\omega) = B(\omega)K(\omega)C_0(\omega)$ . Note that the exact expression of  $U_0(\omega)$  can be obtained from previous work<sup>4,19</sup> but will be useless here.

Equation (10) implies

$$\Delta C_{ij}^{res+}(\omega) = \Delta C_{ij}^+(\omega) e^{j\omega \mathcal{E}_{ij}}. \quad (15)$$

Thus,

$$\Delta C_{ij}^{res+}(\omega) = f(\theta_{ij}, \omega) \chi_{ij} e^{-jk(\omega)d_{ij}} U_0(\omega) e^{j\omega \mathcal{E}_{ij}}. \quad (16)$$

For simplification purposes, we will number the receiver pairs as  $n \equiv (ij)$ .

Next, the backpropagation algorithm is applied for the defect localization. It consists of backpropagating the differential correlation associated with each sensor pair on the distance first sensor-pixel-second sensor. Then, summation over all sensor pairs results in the so-called backpropagation function,<sup>4</sup> expressed in the frequency domain and for pixels located on the defect position as

$$\text{BPF}(\omega) = \sum_{n=1}^{N_c} \Delta C_n^{res+}(\omega) e^{jk(\omega)d_n}, \quad (17)$$

where  $N_c = N^2$  is the number of pairs.

To keep only the first wave packets and remove the reverberations, we return to the time domain via the inverse Fourier transform,  $\text{bpf}(t)$ . Then, we compute the time-windowed intensity on the defect position as follows:

$$I_{res} = \int_{-T_0/2}^{T_0/2} |\text{bpf}(t)|^2 dt, \quad (18)$$

where  $T_0$  is the wave packet duration.

Replacing  $\text{bpf}(t)$  by its expression [inverse Fourier transform of Eq. (17)], we then obtain

$$I_{res} = \int_{-T_0/2}^{T_0/2} \left( \sum_{n=1}^{N_c} f(\theta_n, \omega) \chi_n u_n(t) \right)^2 dt, \quad (19)$$

where  $u_n(t) = u_0(t + \mathcal{E}_n)$ .

Assuming that the defect has isotropic scattering behavior, then  $|f(\theta_n, \omega_0)|^2 = \sigma_0/2\pi$ , where  $\sigma_0$  is the defect scattering cross section<sup>19</sup> at frequency  $\omega_0$ . Equation (19) becomes

$$I_{res} = \frac{\sigma_0}{2\pi} \int_{-T_0/2}^{T_0/2} \left[ \sum_{n=1}^{N_c} \chi_n^2 u_n^2 + \sum_{n=1}^{N_c} \sum_{m \neq n}^{N_c} \chi_n \chi_m u_n(t) u_m(t) \right] dt, \quad (20)$$

which can be written as

$$I_{res} = \frac{\sigma_0}{2\pi} \left[ E_0 \sum_{n=1}^{N_c} \chi_n^2 + \sum_{n=1}^{N_c} \sum_{m \neq n}^{N_c} \chi_n \chi_m \int_{-T_0/2}^{T_0/2} u_n(t) u_m(t) dt \right], \quad (21)$$

where  $E_0 = \int_{-T_0/2}^{T_0/2} u_0^2(t) dt$ .

Because we are interested in an average behavior of the intensity on the defect position, introducing the statistical mean (denoted by  $\langle \cdot \rangle$ ) on  $I_{res}$  for a set of random realizations on  $\mathcal{E}_n$  and knowing that  $u_n(t)$  and  $u_m(t)$  are independent for  $n \neq m$ , we obtain

$$\langle I_{\text{res}} \rangle = \frac{\sigma_0 N_c^2}{2\pi} \left( E_0 \sum_{n=1}^{N_c} \chi_n^2 + E_1 \sum_{n=1}^{N_c} \sum_{m \neq n}^{N_c} \chi_n \chi_m \right), \quad (22)$$

where  $E_1 = \int_{-T_0/2}^{T_0/2} \langle u_n(t) \rangle^2 dt$ .

Defining  $\bar{\chi} = (1/N_c) \sum_{n=1}^{N_c} \chi_n$ , and  $\overline{\chi^2} = (1/N_c) \sum_{n=1}^{N_c} \chi_n^2$ , it is easy to show that  $\sum_{n=1}^{N_c} \sum_{m \neq n}^{N_c} \chi_n \chi_m = N_c^2 \bar{\chi}^2 - N_c \overline{\chi^2}$ , thus

$$\langle I_{\text{res}} \rangle = \frac{\sigma_0 N_c^4}{2\pi} \left[ E_1 \bar{\chi}^2 + \frac{E_0 - E_1}{N_c} \overline{\chi^2} \right]. \quad (23)$$

Considering that  $N_c$  is large enough to neglect  $[(E_0 - E_1)/N_c] \overline{\chi^2}$ ,  $\langle I_{\text{res}} \rangle$  can be approximated as

$$\langle I_{\text{res}} \rangle \approx \frac{\sigma_0 N_c^4}{2\pi} E_1 \bar{\chi}^2. \quad (24)$$

To quantify the degradation of the defect detection as a function of time shift, we define a contrast ratio, denoted  $C_r$ , between the case with resynchronization error and a reference case without resynchronization error as

$$C_r = \frac{\langle I_{\text{res}} \rangle}{I}, \quad (25)$$

where  $I$  is the defect pixel intensity in the case of synchronized signals (the case where  $E_1 = E_0$ ).

According to Eq. (24), the contrast ratio can then be simplified as

$$C_r = \frac{E_1}{E_0}. \quad (26)$$

Using Parseval's theorem,  $E_1$  can be written such that

$$E_1 = \int |FT(\langle u_n(t) \rangle)|^2 d\omega, \quad (27)$$

where  $FT(\cdot)$  denotes the Fourier transform.

From the definition of  $u_n(t)$ , we have  $|FT(\langle u_n(t) \rangle)|^2 = |U_0(\omega)|^2 \times |e^{j\omega \mathcal{E}_n}|^2$ . Using the transfer theorem, we can easily show that

$$\langle e^{j\omega \mathcal{E}_n} \rangle = \int e^{j\omega \mathcal{E}} p(\mathcal{E}) d\mathcal{E}, \quad (28)$$

which is simply  $\sqrt{2\pi}$  times the Fourier transform,  $p(\omega)$ , of the probability density function of  $\mathcal{E}$ .

Thus, Eq. (27) yields

$$E_1 = 2\pi \int |U_0(\omega)|^2 \times |p(\omega)|^2 d\omega. \quad (29)$$

Assuming that the standard deviation of  $\mathcal{E}$  is small compared to the wave propagation time, the probability density function,  $p(\mathcal{E})$ , is a narrow time-dependent function. This implies that its Fourier transform,  $p(\omega)$ , evolves slowly over the

frequency band of  $U_0(\omega)$ . Then,  $\int |U_0(\omega)|^2 \times |p(\omega)|^2 d\omega = |p(\omega_0)|^2 E_0$ , and by introducing Eq. (29) into Eq. (26), we finally obtain

$$C_r \approx 2\pi |p(\omega_0)|^2, \quad (30)$$

where  $\omega_0$  is the central frequency of the bandwidth.

This expression shows how localization performance is related to the standard deviation of the resynchronization error. It will be applied and validated in a numerical case in Sec. IV. However, first, we will show in Sec. III how this standard deviation can be minimized by applying a mathematical manipulation based on Moore-Penrose pseudo-inversion, thus resulting in improved contrast ratio.

### III. MINIMIZATION OF RESYNCHRONIZATION ERRORS USING A MOORE-PENROSE PSEUDO-INVERSE PROCESS

As explained in Sec. II, the time shifts,  $\delta_n$ , of the noise correlation functions are obviously the direct consequence of the individual receiver's time drifts,  $\Delta_i$  [see Eq. (5)]. Yet, the PCT-based method has consisted of estimating and then compensating, directly, the  $\delta_n$  without caring about the original drifts. Although this is in principle sufficient for successful application of the localization algorithm, we will see here that recovering the set of  $\Delta_i$  by pseudo-inversion of Eq. (5) will have a regularization effect on the correlation time shift estimations.

First, Eq. (5) can be written in matrix form as

$$\delta = M\Delta, \quad (31)$$

where  $M$  is a connectivity matrix of dimension  $(N_c \times N)$  containing 1, 0, and  $-1$  elements.  $\Delta$  is a vector of  $(N \times 1)$  elements containing time drifts,  $\Delta_i$ , of the  $N$  sensors. Finally,  $\delta$  is the  $(N_c \times 1)$  vector of the correlation shifts,  $\delta_n$ .

Similarly, Eq. (8) can be written in matrix form as  $\delta_e = \delta + \mathcal{E}$ , where  $\mathcal{E}$  is the vector of estimation errors. From these estimated correlation shifts,  $\delta_e$ , we can then estimate a time drift vector,  $\Delta_p$ , through a pseudo-inversion as follows:

$$\Delta_p = M^+ \delta_e, \quad (32)$$

where  $M^+$  is the Moore-Penrose pseudo-inverse<sup>20</sup> of  $M$ , and the index,  $p$ , refers to *pseudo-inverse*.

$\Delta_p$  corresponds to the  $N$  receiver clock drifts best matching (in the least-square sense) the correlation shifts that could be estimated experimentally through the PCT method. Next, we can multiply it by matrix,  $M$ , to obtain a constrained version of these correlation shifts as

$$\delta_p = M\Delta_p = MM^+ \delta_e. \quad (33)$$

According to Eq. (31), Eq. (33) becomes

$$\delta_p = MM^+ M\Delta + MM^+ \mathcal{E}. \quad (34)$$

As well-known properties of the Moore-Penrose pseudo-inverse imply that  $MM^+ M = M$ , Eq. (33) yields

$$\delta_p = \delta + \mathcal{E}_p, \tag{35}$$

where  $\mathcal{E}_p = A \mathcal{E}$  and  $A = MM^+$ .

This process then provides us with a new set of estimated correlation shifts,  $\delta_p$ , with resynchronization errors,  $\mathcal{E}_p$ , whose variance can be written as

$$\sigma_p^2 = \frac{\langle \mathcal{E}_p^T \mathcal{E}_p \rangle}{N_c}, \tag{36}$$

where  $\mathcal{E}_p^T$  denotes the transpose of  $\mathcal{E}_p$  and  $\langle \cdot \rangle$  denotes the mathematical expectation for a set of random realizations on  $\mathcal{E}_p$ .

In the same way, the variance of the initial synchronization error,  $\mathcal{E}$ , of the originally estimated shifts,  $\delta_e$ , is

$$\sigma^2 = \frac{\langle \mathcal{E}^T \mathcal{E} \rangle}{N_c}. \tag{37}$$

Substituting  $\mathcal{E}_p$  by its previously defined expression yields

$$\mathcal{E}_p^T \mathcal{E}_p = \mathcal{E}^T (M^+)^T M^T M M^+ \mathcal{E}. \tag{38}$$

Knowing that  $(M^+)^T M^T = (MM^+)^T = MM^+$  and  $MM^+ M = M$  (pseudo-inverse and transpose properties), Eq. (38) becomes

$$\mathcal{E}_p^T \mathcal{E}_p = \mathcal{E}^T A \mathcal{E}. \tag{39}$$

By decomposing  $A$  into a sum of diagonal [ $\text{diag}(A)$ ] and off diagonal [ $\text{odiag}(A)$ ] matrices, Eq. (39) becomes

$$\mathcal{E}_p^T \mathcal{E}_p = \mathcal{E}^T \text{diag}(A) \mathcal{E} + \mathcal{E}^T \text{odiag}(A) \mathcal{E}. \tag{40}$$

Then, taking the expected value of Eq. (40), the second term cancels out because it contains only cross-independent terms.

As for the first term, its expected value yields  $\langle \mathcal{E}^T \text{diag}(A) \mathcal{E} \rangle = \sigma^2 \text{Tr}(A)$ , where  $\text{Tr}(A)$  is the trace of matrix  $A$ . Because Moore-Penrose pseudo-inverse properties imply that  $\text{Tr}(A) = \text{rank}(M) = N - 1$ , Eq. (40) yields

$$\langle \mathcal{E}_p^T \mathcal{E}_p \rangle = \sigma^2 (N - 1). \tag{41}$$

Introducing Eq. (41) into Eq. (36) finally yields

$$\sigma_p = \frac{\sqrt{N - 1}}{N} \sigma. \tag{42}$$

This means that the standard deviation of the resynchronization error is reduced by a factor of  $\sqrt{N - 1}/N$  when applying the pseudo-inverse process proposed here.

#### IV. NUMERICAL VALIDATION AND DISCUSSION

To validate the theoretical expressions developed in Secs. II and III, a simple numerical simulation is performed in this section.

We consider the propagation of flexural waves in an infinite plate with no absorption. In the frequency domain, this propagation between a source and a receiver,  $R_i$ , at positions  $\vec{r}_s$  and  $\vec{r}_i$ , respectively, can be modeled in the far-field through the following propagation function:

$$P(\vec{r}_s, \vec{r}_i, \omega) = \frac{1}{\sqrt{\|\vec{r}_s - \vec{r}_i\|}} e^{-jk(\omega)\|\vec{r}_s - \vec{r}_i\|}, \tag{43}$$

where  $k(\omega)$  is the wave number of flexural waves.

Therefore, the received signal at  $R_i$  can be expressed as

$$u(\vec{r}_s, \vec{r}_i, \omega) = P(\vec{r}_s, \vec{r}_i, \omega) \times u_e(\omega), \tag{44}$$

where  $u_e(\omega)$  is the Fourier transform of the emission signal.

In the presence of a defect, the signal received at  $R_i$  can be written such that

$$u_d(\vec{r}_s, \vec{r}_i, \omega) = u(\vec{r}_s, \vec{r}_i, \omega) + \Delta u(\vec{r}_s, \vec{r}_i, \omega), \tag{45}$$

where  $\Delta u(\vec{r}_s, \vec{r}_i, \omega) = f_d(\vec{r}_s, \vec{r}_i, \omega) \times P(\vec{r}_s, \vec{r}_d, \omega) \times u(\vec{r}_s, \vec{r}_d, \omega)$ , where  $f_d(\vec{r}_s, \vec{r}_i)$  is the defect scattering amplitude, and  $\vec{r}_d$  is the defect position.

Using the inverse Fourier transform, we return to the time domain to obtain the signals  $u_d(\vec{r}_s, \vec{r}_i, t)$  and  $u(\vec{r}_s, \vec{r}_i, t)$  received by  $R_i$  in both cases: with and without defect, respectively.

The tested configuration (see Fig. 2) consists of an infinite 3-mm-thick aluminum plate of physical properties: Young's modulus,  $E = 70$  GPa; volume density,  $\rho = 2700$  kg/m<sup>3</sup>; and Poisson's ratio,  $\nu = 0.35$ . Eight receivers (blue crosses) are placed at known positions over its surface. The origin is taken at the center of the array of receivers. At position (2, 1) cm, a defect is modeled by a point scatterer with constant  $f_d$  (isotropic scatterer). A set of 500 sources (red dots) are randomly distributed around the receivers.

The emission signal is a one-cycle Hanning-windowed sine of frequency  $f_0 = 20$  kHz. The sampling frequency is 1.5 MS/s. For each pair of receivers, the summed cross correlation over all sources is computed (an example is displayed in Fig. 3).

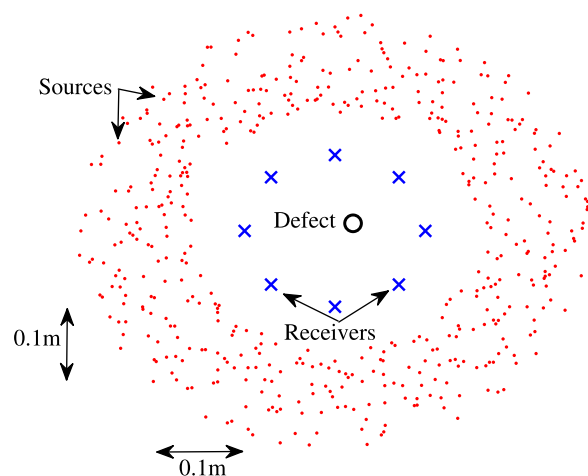


FIG. 2. (Color online) Schematic representation of the simulated configuration.

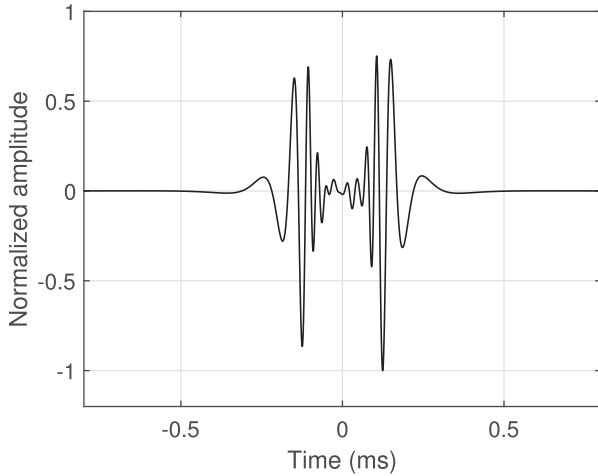


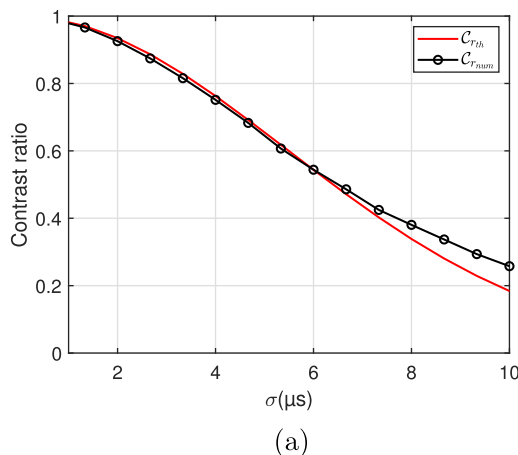
FIG. 3. Example of a cross correlation summed over all sources and normalized with respect to the maximum value.

The backpropagation-based imaging algorithm recalled in Sec. II is then applied on the positive time lag of computed differential cross correlations. The obtained localization image for an area of  $(40 \times 40) \text{ cm}^2$  around the defect is depicted in Fig. 4. Pixel intensities are normalized with respect to the maximum intensity. As expected, the defect location is correctly localized.

Now, we are interested in highlighting the effect of synchronization errors on the defect localization image quality. These errors are modeled by random shifts following a Gaussian distribution,  $\mathcal{N}(0, \sigma)$ , which is introduced on the computed cross correlations. For each value of  $\sigma$ , the contrast ratio between the cases with and without synchronization errors is computed and averaged over 500 realizations. This averaged numerical contrast ratio can then be compared to the theoretical expression established in Sec. II [see Eq. (30)].

In this case of a Gaussian distribution, the Fourier transform of the probability density function is

$$p(\omega) = \frac{1}{\sqrt{2\pi}} e^{-\sigma^2 \omega^2 / 2}. \quad (46)$$



(a)

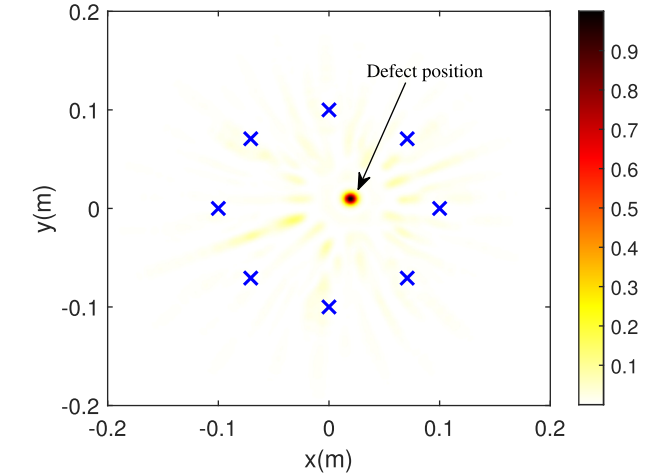


FIG. 4. (Color online) Defect localization image.

Consequently, Eq. (30) in Sec. II becomes

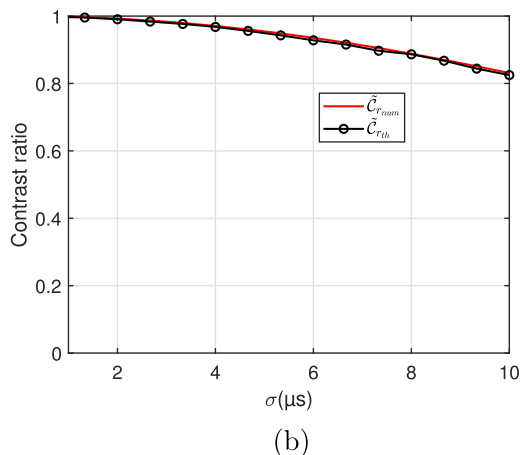
$$C_r = e^{-\sigma^2 \omega_0^2}. \quad (47)$$

If the Moore-Penrose pseudo-inverse process is applied, then, according to Eq. (42), the contrast ratio becomes

$$\tilde{C}_r = e^{[-(N-1)\sigma^2/N^2]\omega_0^2}. \quad (48)$$

The corresponding curves as a function of  $\sigma$  are represented in Fig. 5 along with the averaged numerical contrast ratios computed from the simulation.

First, referring to Fig. 5(a), the numerical contrast ratio (red circles) matches the theoretical prediction (black line) for small values of  $\sigma$  ( $\sigma \leq 7 \mu\text{s}$ ). Above  $7 \mu\text{s}$ , we notice a discrepancy of the numerical curve compared to the theoretical curve. This is due to the assumption of low sigma values used in Sec. II. Finally, from Fig. 5(b), it is clear that the Moore-Penrose pseudo-inversion leads to a significant improvement in the contrast ratio subsequent to the minimization of the standard deviation of the resynchronization error.



(b)

FIG. 5. (Color online) Comparison between numerical (black circles) and theoretical (red line) contrast ratios in the cases (a) without and (b) with applying Moore-Penrose pseudo-inverse process.



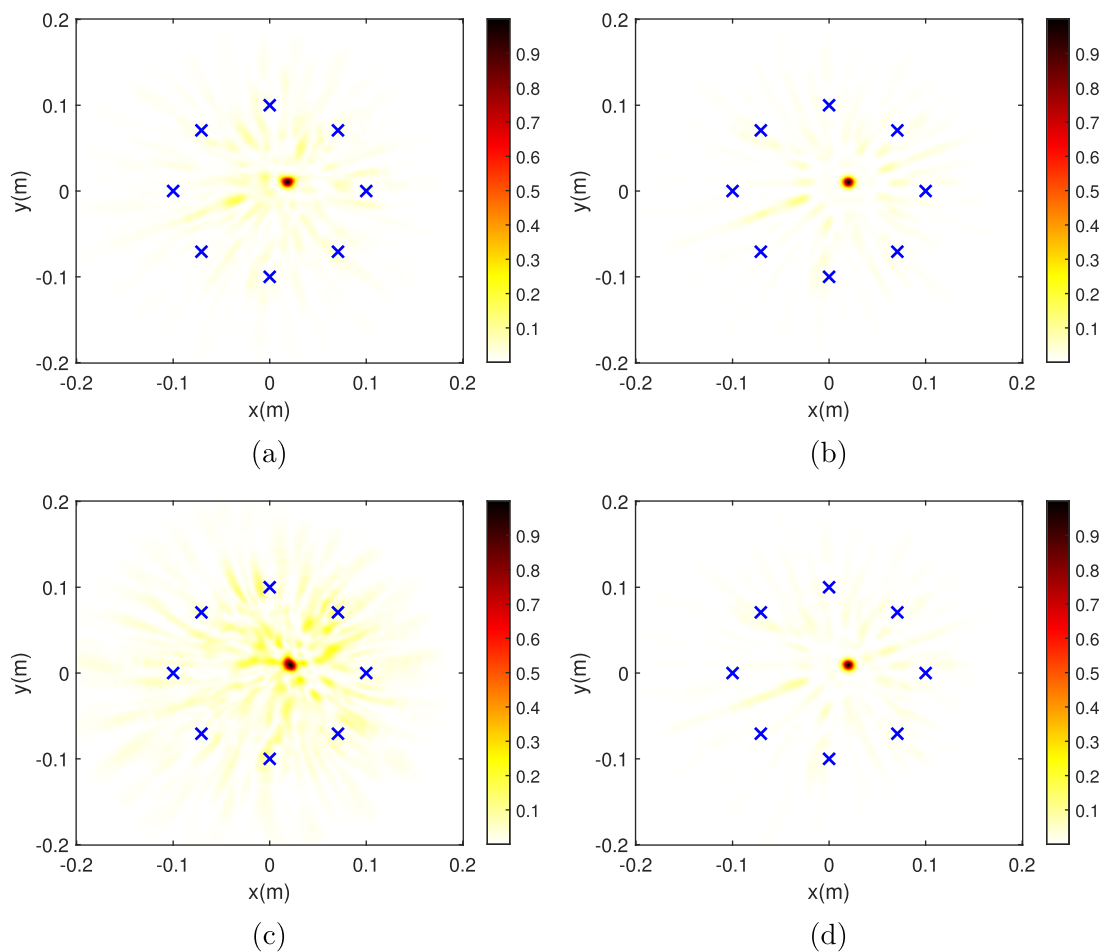


FIG. 6. (Color online) Comparison between localization images in the case of [(a) and (b)]  $\sigma = 7 \mu\text{s}$ , [(c) and (d)]  $\sigma = 12 \mu\text{s}$ , [(a) and (c)] without and [(b) and (d)] with applying the Moore-Penrose pseudo-inverse process.

This improvement effect brought by the Moore-Penrose pseudo-inversion on the quality of the defect localization is highlighted in Fig. 6. Two examples of localization images [Figs. 6(a) and 6(c)] without and [Figs. 6(b) and 6(d)] with applying the regularization process for standard deviations of the resynchronization errors  $\sigma = 7 \mu\text{s}$  and  $\sigma = 12 \mu\text{s}$  are presented.

As expected, the reduction of resynchronization errors leads to a significant improvement of the localization images quality.

## V. CONCLUSION

This paper deals with the problem of possibly imperfect signal resynchronization for passive imaging based on noise correlation in plate-like structures when acoustic sensors with independent timebases are used.

Theoretical developments have been performed to quantify the degradation of the contrast ratio of defect localization images as a function of the statistical properties of the resynchronization errors of the correlation functions. A simple numerical simulation has been performed to validate the obtained theoretical expression of contrast ratio versus standard deviation of resynchronization errors. In addition, it has been revealed

how this standard deviation can be significantly reduced by applying a suitable pseudo-inverse processing. This allows to maintain satisfying detection contrast even when correlation functions are imperfectly resynchronized. This work can be of great interest for SHM applications using, possibly, wireless acoustic sensor networks.

Future work will focus, in particular, on the effect of measurement noise, sources distribution, and residual synchronization errors caused by imperfect Green's function reconstruction.

## AUTHOR DECLARATIONS

### Conflict of Interest

The authors have no conflicts to disclose.

## DATA AVAILABILITY

The data that support the findings of this study are available from the corresponding author upon reasonable request.

## NOMENCLATURE

### SYMBOLS OF ENGLISH ALPHABET

$B$  Source function

BPF	Back propagation function
$C$	Cross correlation
$C^{\text{mes}}$	measured cross correlation
$C^{\text{res}}$	resynchronized cross correlation
$C_0$	Ambient noise auto correlation
$\tilde{C}_r$	Contrast ratio
$\tilde{\tilde{C}}_r$	Contrast ratio after applying the Moore-Penrose pseudo-inversion process
$G$	Green's function
$I$	Pixel intensity computed on the defect position using synchronized cross correlations
$I_{\text{res}}$	Pixel intensity computed on the defect position using resynchronized cross correlations
$s^{\text{mes}}$	Measured signal
$M$	Connectivity matrix
$M^+$	Moore-Penrose pseudo-inverse of $M$
$N$	Number of sensors
$N_c$	Number of sensor pairs
$p$	Probability density function of resynchronization errors

### Symbols of Greek alphabet

$\delta$	Correlation's time shift
$\Delta$	Sensor's time drift
$\mathcal{E}$	Resynchronization error
$\mathcal{E}_p$	Resynchronization error after applying the Moore-Penrose pseudo-inversion process
$\omega_0$	Central frequency of the bandwidth
$\sigma$	Standard deviation of resynchronization errors
$\sigma_0$	Defect scattering cross section
$\sigma_p$	Standard deviation of resynchronization errors after applying the Moore-Penrose pseudo-inversion process
$\chi$	Geometric factor

<sup>1</sup>M. Abbas and M. Shafiee, "Structural health monitoring (SHM) and determination of surface defects in large metallic structures using ultrasonic guided waves," *Sensors* **18**(11), 3958 (2018).

<sup>2</sup>O. I. Lobkis and R. L. Weaver, "On the emergence of the Green's function in the correlations of a diffuse field," *J. Acoust. Soc. Am.* **110**, 3011–3017 (2001).

<sup>3</sup>A. Colombi, L. Boschi, P. Roux, and M. Campillo, "Green's function retrieval through cross-correlations in a two-dimensional complex reverberating medium," *J. Acoust. Soc. Am.* **135**(3), 1034–1043 (2014).

<sup>4</sup>L. Chehami, E. Moulin, J. de Rosny, C. Prada, O. Bou Matar, F. Benmeddour, and J. Assaad, "Detection and localization of a defect in a reverberant plate using acoustic field correlation," *J. Appl. Phys.* **115**(10), 104901 (2014).

<sup>5</sup>L. Chehami, J. de Rosny, C. Prada, E. Moulin, and J. Assaad, "Experimental study of passive defect localization in plates using ambient noise," *IEEE Trans. Ultrason., Ferroelect., Freq. Contr.* **62**(8), 1544–1553 (2015).

<sup>6</sup>A. Hejazi Nooghabi, L. Boschi, P. Roux, and J. De Rosny, "Coda reconstruction from cross-correlation of a diffuse field on thin elastic plates," *Phys. Rev. E* **96**(3), 032137 (2017).

<sup>7</sup>L. Sadoudi, M. Bocquet, E. Moulin, and J. Assaad, "ZigBee sensor network platform for health monitoring of rails using ambient noise correlation," *J. Electr. Eng.* **5**(3), 143–150 (2017).

<sup>8</sup>C. B. Nzouatchoua, M. Bentahar, S. Montesor, N. Colin, V. Le Cam, C. Trottier, and N. Terrien, "Damage localization on composite structures based on the delay-and-sum algorithm using simulation and experimental methods," *Sensors* **23**(9), 4368 (2023).

<sup>9</sup>L. Arceo-Miquel, Y. S. Shmaliy, and O. Ibarra-Manzano, "Optimal synchronization of local clocks by GPS 1PPS signals using predictive FIR filters," *IEEE Trans. Instrum. Meas.* **58**(6), 1833–1840 (2009).

<sup>10</sup>I. Rhee, J. Lee, J. Kim, E. Serpedin, and Y. Wu, "Clock synchronization in wireless sensor networks: An overview," *Sensors* **9**(1), 56–85 (2009).

<sup>11</sup>J. Elson, L. Girod, and D. Estrin, "Fine-grained network time synchronization using reference broadcasts," *SIGOPS Oper. Syst. Rev.* **36**(SI), 147–163 (2002).

<sup>12</sup>B. Sundararaman, U. Buy, and A. D. Kshemkalyani, "Clock synchronization for wireless sensor networks: A survey," *Ad Hoc Netw.* **3**(3), 281–323 (2005).

<sup>13</sup>C. Sens-Schönfelder, "Synchronizing seismic networks with ambient noise," *Geophys. J. Int.* **174**(3), 966–970 (2008).

<sup>14</sup>L. Stehly, M. Campillo, and N. M. Shapiro, "Traveltime measurements from noise correlation: Stability and detection of instrumental time-shifts," *Geophys. J. Int.* **171**(1), 223–230 (2007).

<sup>15</sup>K. G. Sabra, P. Roux, A. M. Thode, G. L. D'Spain, W. S. Hodgkiss, and W. A. Kuperman, "Using ocean ambient noise for array self-localization and self-synchronization," *IEEE J. Ocean. Eng.* **30**(2), 338–347 (2005).

<sup>16</sup>A. M. Thode, P. Gerstoft, W. C. Burgess, K. G. Sabra, M. Guerra, M. D. Stokes, M. Noad, and D. H. Cato, "A portable matched-field processing system using passive acoustic time synchronization," *IEEE J. Ocean. Eng.* **31**(3), 696–710 (2006).

<sup>17</sup>P. Gouedard, T. Seher, J. J. McGuire, J. A. Collins, and R. D. van der Hilst, "Correction of ocean-bottom seismometer instrumental clock errors using ambient seismic noise," *Bull. Seismol. Soc. Am.* **104**(3), 1276–1288 (2014).

<sup>18</sup>L. Chehami, E. Moulin, J. De Rosny, and C. Prada, "Accuracy of Green's function estimation from correlation of diffuse elastic waves on thin plates," *J. Acoust. Soc. Am.* **146**(5), 3505–3511 (2019).

<sup>19</sup>H. Achdjian, E. Moulin, F. Benmeddour, J. Assaad, L. Dupont, and L. Chehami, "Reverberation of flexural waves scattered by a local heterogeneity in a plate," *J. Acoust. Soc. Am.* **140**(1), 157–164 (2016).

<sup>20</sup>J. Jang, D. Kim, and I. Kim, "Singularity handling for unbalanced three-phase transformers in Newton-Raphson power flow analyses using Moore-Penrose pseudo-inverse," *IEEE Access* **11**, 40657–40674 (2023).